REPORT

FLEXIBLE ELECTRONICS

Highly stretchable polymer semiconductor films through the nanoconfinement effect

Jie Xu,[1]* Sihong Wang,[1]* Ging-Ji Nathan Wang,[1] Chenxin Zhu,[2] Shaochuan Luo,[3] Lihua Jin,[4,5] Xiaodan Gu,[1,6]† Shucheng Chen,[1] Vivian R. Feig,[7] John W. F. To,[1] Simon Rondeau-Gagné,[1]‡ Joonsuk Park,[7] Bob C. Schroeder,[1]§ Chien Lu,[1] Jin Young Oh,[1] Yanming Wang,[7] Yun-Hi Kim,[8] He Yan,[9] Robert Sinclair,[7] Dongshan Zhou,[3] Gi Xue,[3] Boris Murmann,[2] Christian Linder,[5] Wei Cai,[4] Jeffery B.-H. Tok,[1] Jong Won Chung,[1,10]|| Zhenan Bao[1]||

Soft and conformable wearable electronics require stretchable semiconductors, but existing ones typically sacrifice charge transport mobility to achieve stretchability. We explore a concept based on the nanoconfinement of polymers to substantially improve the stretchability of polymer semiconductors, without affecting charge transport mobility. The increased polymer chain dynamics under nanoconfinement significantly reduces the modulus of the conjugated polymer and largely delays the onset of crack formation under strain. As a result, our fabricated semiconducting film can be stretched up to 100% strain without affecting mobility, retaining values comparable to that of amorphous silicon. The fully stretchable transistors exhibit high biaxial stretchability with minimal change in on current even when poked with a sharp object. We demonstrate a skinlike finger-wearable driver for a light-emitting diode.

Electronics for biomedical applications, such as physiological monitoring (*1*), implanted treatment (*2*), electronic skins (*3*), and human-machine interface (*4*), must be mechanically compatible with biological tissues, with characteristics of low modulus, flexibility, and stretchability. Several approaches based on geometric designs, such as buckles (*5*), wavy patterns (*1*, *2*), and kirigami (*6*), impart stretchability to electronics and have the potential for a variety of wearable applications. Stretchable electronics based on intrinsically stretchable materials may enable scalable fabrication, higher device density, and better strain tolerance but remain scarce owing to the lack of high-performance stretchable semiconductors that possess both high mechanical ductility and high carrier mobility at large strains. Although some nanomaterial systems [such as two-dimensional (2D) materials] possess moderate stretchability (below 20% strain) with good electrical performance (*7*), their rigid nature has limited device density, mechanical robustness, and wide applicability.

Conjugated polymers have been developed as a softer semiconductor with high charge carrier mobilities rivaling that of poly-Si (*8*–*10*), but their stretchability remains poor. Molecular design rules (*11*–*14*) that are effective in improving stretchability often result in a decrease in mobility. Nanowire and nanofibril networks (*15*, *16*) and microcracked films (*17*) improved strain tolerance, but the materials used were already known to be ductile (*18*) and had low mobilities. More recently, high-performance but brittle conjugated polymers have been afforded improved stretchability through blending with a ductile lower-performance conjugated polymer (*19*). However, the films still have limited ductility due to the unchanged polymer chain packing and dynamics.

Nanoconfinement of polymers into nanometer-scale dimensions is known to result in peculiar thermodynamic and kinetic properties due to the finite-size effect and the interface effect. Nanoconfinement can alter many polymer physical properties, including lowering the mechanical modulus (*20*) and glass transition temperature (*21*) and increasing the mechanical ductility (*22*). These changes have been attributed to the enhanced polymer chain dynamics in the amorphous regions (*23*, *24*) and the restricted growth of large crystallites (*25*), and these are all desirable for stretchable materials. Therefore, we hypothesized that the increased polymer chain dynamics and suppressed crystallization from nanoconfinement may increase the mechanical stretchability of high-mobility, less ductile polymer semiconductors.

Nanoconfinement of polymer semiconductor is achieved by forming nanofibrils inside a soft, deformable elastomer (Fig. 1A). Good charge transport is maintained owing to the connectivity between the nanofibril aggregates, while their interfacing with the deformable elastomer prevents crack propagation. Possible fabrication techniques include photolithographic patterning (*26*), nanostructure templating (*27*), and phase separation (*28*), but only the latter method can simultaneously introduce all desirable features in one step, is more scalable, and can be achieved at low cost. We describe a conjugated-polymer/elastomer phase separation–induced elasticity (termed CONPHINE) methodology to achieve the desired morphology.

We first investigate poly(2,5-bis(2-octyldodecyl)-3,6-di(thiophen-2-yl)diketopyrrolo[3,4-c]pyrrole-1,4-dione-alt-thieno[3,2-b]thiophen) (DPPT-TT; **1**) (table S1) (*29*) as the high-mobility semiconducting polymer and polystyrene-*block*-poly(ethylene-*ran*-butylene)-*block*-polystyrene (SEBS) as the soft elastomer (Fig. 1B). Their comparable surface energies should ensure a nanoscale mixed morphology (fig. S1 and table S2). The improvement in mechanical ductility is investigated on three model films of **1**: (i) thick neat film (~135 nm), (ii) thin neat film (~35 nm) with the nanoconfinement effect, and (iii) thin film/SEBS bilayer film with both the nanoconfinement effect and a deformable interface (Fig. 1C). As an important parameter representing the polymer chain dynamics, the glass transition temperatures (T_g) of DPPT-TT obtained by the differential AC chip calorimetric method show a decreasing trend from the thick, to the thin, and finally to the nanofiber (obtained by removing SEBS from the CONPHINE film) films (Fig. 1D and fig. S2). This trend confirms increased chain dynamics due to nanoconfinement (*21*, *23*, *24*). Suppressed crystallization in thinner films (*25*) was also observed (Fig. 1E and fig. S3). These two effects together result in a decrease in the measured elastic modulus and a significant increase in the onset strains of plasticity and cracks from thick to thin film (Fig. 1F and figs. S4 to S6) (*20*, *22*, *30*). Under 2D nanoconfinement, the simulated modulus of the DPPT-TT nanofiber is one-half that of the bilayer film and almost one-sixth that of the thick film (Fig. 1F and fig. S7). The introduction of the SEBS deformable interface further decreases the

[1]Department of Chemical Engineering, Stanford University, Stanford, CA 94305, USA. [2]Department of Electrical Engineering, Stanford University, Stanford, CA 94305, USA. [3]Department of Polymer Science and Engineering, School of Chemistry and Chemical Engineering, Nanjing University, Nanjing 210093, China. [4]Department of Mechanical Engineering, Stanford University, Stanford, CA 94305, USA. [5]Department of Civil and Environmental Engineering, Stanford University, Stanford, CA 94305, USA. [6]Stanford Synchrotron Radiation Lightsource, SLAC National Accelerator Laboratory, Menlo Park, CA 94025, USA. [7]Department of Materials Science and Engineering, Stanford University, Stanford, CA 94305, USA. [8]Department of Chemistry and RINS, Gyeongsang National University, Jinju 660-701, South Korea. [9]Department of Chemistry and Hong Kong Branch of Chinese National Engineering Research Center for Tissue Restoration & Reconstruction, The Hong Kong University of Science and Technology, Clear Water Bay, Kowloon, Hong Kong. [10]Samsung Advanced Institute of Technology Yeongtong-gu, Suwon-si, Gyeonggi-do 443-803, South Korea.
*These authors contributed equally to this work. †Present address: School of Polymer Science and High Performance Materials, University of Southern Mississippi, Hattiesburg, MS 39402, USA. ‡Present address: Department of Chemistry and Biochemistry, University of Windsor, Windsor, Ontario N9B 3P4, Canada. §Present address: Materials Research Institute and School of Biological and Chemical Sciences, Queen Mary University London, Mile End Road, London E1 4NS, UK. ||Corresponding author. Email: zbao@stanford.edu (Z.B.); jw0903.chung@samsung.com (J.W.C.)

crystallinity (Fig. 1E) and reduces crack propagation, which makes the bilayer film further softened and more ductile (Fig. 1F and figs. S4 to S6). The improvement in stretchability from these effects is shown by both the dichroic ratios (from ultraviolet/visible spectroscopy) (fig. S8) and substantially different crack size of these films under strain (fig. S9).

As observed by the atomic force microscopy (AFM) phase images, the CONPHINE-**1** film showed the desired fiber network with smaller nanofiber diameters at higher SEBS concentrations (fig. S10). At 70 weight % (wt %) of SEBS, the nanofiber diameter became small enough (<50 nm) to give a strong nanoconfinement effect at both the top and bottom surfaces (Fig. 1G). As revealed by x-ray photoelectron spectroscopy (XPS) (fig. S11), the layer between the top and bottom surfaces is primarily occupied by SEBS, containing a small amount of DPPT-TT. This morphology is depicted in Fig. 1H. Unlike the pregrown nanowires and nanofibers (*15*, *16*), the

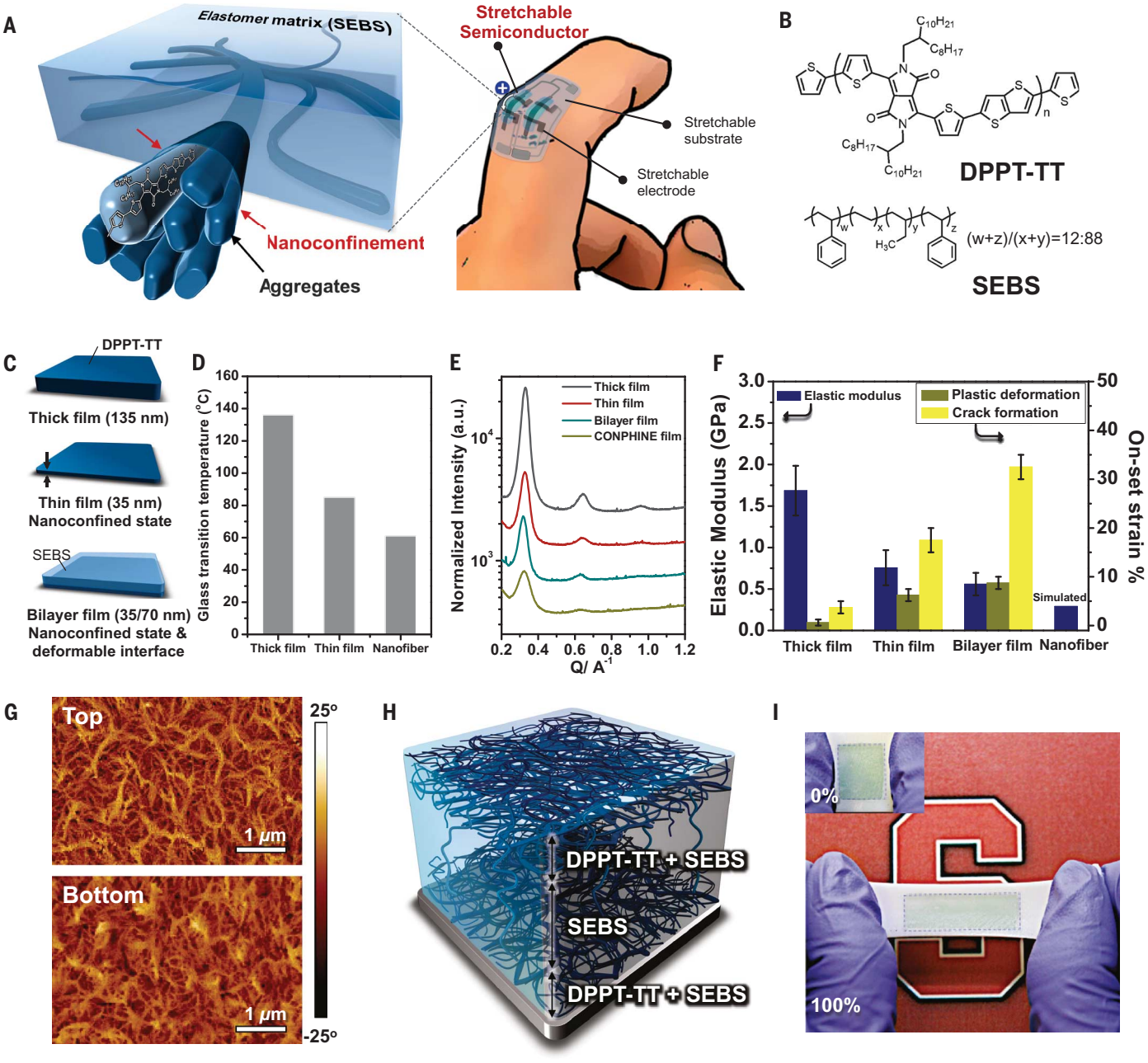

Fig. 1. Nanoconfinement effect for enhancing the stretchability of polymer semiconducting film through the CONPHINE method. (**A**) A 3D schematic of the desired morphology composed of embedded nanoscale networks of polymer semiconductor to achieve high stretchability, which can be used to construct a highly stretchable and wearable TFT. (**B**) Chemical structures of semiconducting polymer DPPT-TT (labeled as **1**) and SEBS elastomer. (**C**) Three model films of DPPT-TT for investigation of the nanoconfinement effect (i.e., increased chain dynamics and suppressed crystallization). (**D**) Glass transition temperatures of the thick, thin, and nanofiber films. (**E**) XRD line cuts for three model films and the CONPHINE-**1** with 70% SEBS film along the q_{xy} axes, normalized by the exposure time and volume of DPPT-TT layer and offset for clarity. (**F**) Elastic moduli, onset strains of plasticity, and onset strains of crack of the model films, with the simulated modulus of the nanofiber film. The error bars of elastic moduli and onset strains represent the standard deviation and the range of measurement error, respectively. (**G**) AFM phase images of the top and bottom interfaces of the CONPHINE-**1** film with 70 wt % SEBS. (**H**) A 3D illustration of the morphology of the CONPHINE-**1** film. (**I**) Photographs of a CONPHINE-**1** film (blue area) at 0% strain and stretched to 100% strain on a rubber substrate.

nanofibers formed from phase separation have reduced crystallinity but still high aggregation (fig. S12), which ensures both enhanced stretchability and good charge transport. The CONPHINE-**1** film can be stretched up to 100% strain when supported on a rubbery substrate without any visible cracks (Fig. 1I). An additional benefit of the CONPHINE method is the reduced consumption of conjugated polymers and transparent film.

The stretchability of the CONPHINE-**1** film is studied by applying 100% strain on a polydimethylsiloxane (PDMS)–supported film (Fig. 2A), then transferring the CONPHINE-1 film to a Si substrate for morphology characterization. The CONPHINE-**1** film with 70% SEBS can be effectively stretched to 100% strain without resulting in any cracks even at the nanoscale, as characterized by AFM (Fig. 2B and fig. S13A), despite inhomogeneity in film thickness after deformation (fig. S13B). In comparison, the neat-**1** film at 100% strain developed cracks with widths around 20 μm (Fig. 2B).

The electrical performance of the CONPHINE-**1** film functioning as a stretchable semiconductor was measured in a thin-film transistor (TFT) by soft contact lamination (*13*) on a bottom-gate–bottom-contact stack: octadecyltrimethoxysilane (OTS)–assembled SiO_2 (gate dielectric)–coated highly doped Si (gate), with Au contacts on the top (Fig. 2C and fig. S14). Because the DPPT-TT nanofibers on the bottom surface of the CONPHINE film are exposed, good ohmic contacts can be formed with the Au electrodes (fig. S15). The CONPHINE film can be prepared on a wafer scale with good uniformity in electrical performance (fig. S16). By comparing the mobility from the CONPHINE-**1** film with different SEBS contents, it was determined that 70 wt % SEBS provides the optimum condition for enabling the highest mobility at 100% strain (fig. S17). As shown in Fig. 2D(i), the CONPHINE-**1** film (i.e., 70 wt % SEBS) displays a transfer property similar to that of the neat-**1** film (i.e., 0% SEBS), which demonstrates that this approach does not sacrifice the semiconductor's electrical performance. When both films were stretched to 100% strain parallel to charge transport, the transfer curve of the CONPHINE film remained unaffected, with its on

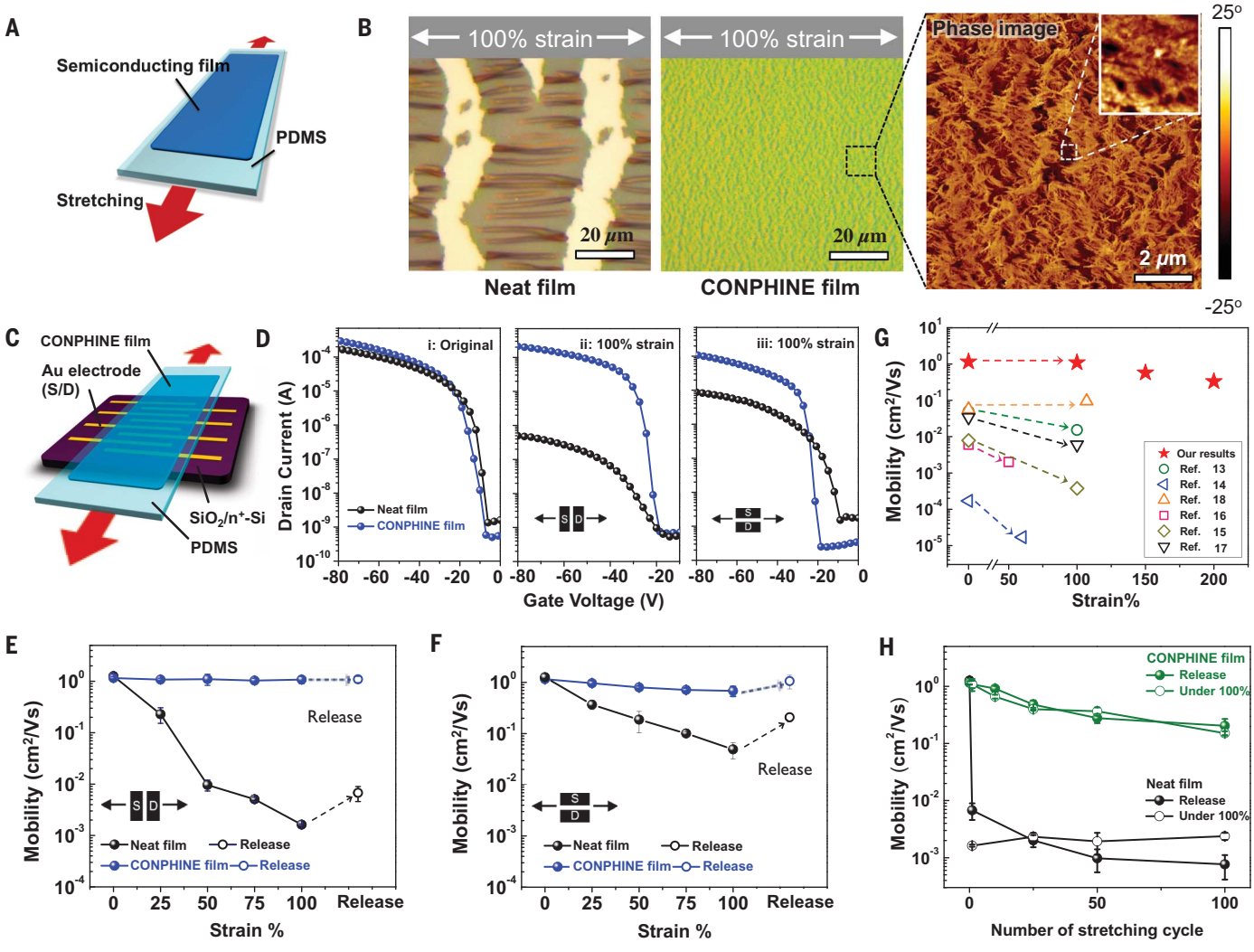

Fig. 2. Characterization of the semiconducting film stretchability and electrical performance under different strains. (**A**) Schematic illustration of the stretching of the semiconducting film supported on PDMS substrate. (**B**) Optical microscope images of a neat-**1** film (left) and a CONPHINE-**1** film (middle) under 100% strain, with an AFM phase image (right) showing that the color variation in CONPHINE-**1** film is not due to cracks. (**C**) Schematic of the soft contact lamination method for characterizing the electrical performance of a semiconducting layer upon stretching. (**D**) Transfer curves (V_D = −80 V, with V_D representing drain voltage) obtained from the CONPHINE-**1** film and the neat-**1** film in its original condition (i), under 100% strain parallel to the charge transport direction (ii), and under 100% strain perpendicular to the charge transport direction (iii). (**E** and **F**) Mobilities from the CONPHINE-**1** film (blue) and the neat-**1** film (black) at different strains (E) parallel and (F) perpendicular to the charge transport direction. (**G**) Comparison of the obtained mobilities at stretched strains in this study to previously reported results in the literature. (**H**) Mobilities of the CONPHINE-**1** film (green) and the neat-**1** film (black) as a function of 100% strain stretching cycles parallel to the charge transport direction.

current ~3 orders of magnitude higher than that of the severely degraded neat-**1** film [Fig. 2D(ii) and fig. S18, A and B]. In addition, the CONPHINE-**1** film showed no decrease in mobility during the entire stretching process (Fig. 2E), in which its mobility at 100% strain reached a maximum value of 1.32 $cm^2/V{\cdot}s$, and 1.08 $cm^2/V{\cdot}s$ on average, which is a ~3-order-of-magnitude improvement compared to the neat-**1** film. When the stretching was perpendicular to the charge transport direction, we observed only a very small decrease in both the on current and the mobility from the CONPHINE-**1** film at 100% strain (Fig. 2, D(iii) and F). This, too, is a marked improvement compared to the ~2-orders-of-magnitude decrease in the neat film. To further probe the film's stretchability, we observed that the CONPHINE-**1** film can even be stretched to 200% strain, with its mobility maintained at 0.33 $cm^2/V{\cdot}s$ (Fig. 2G and fig. S19).

For the CONPHINE-**1** film, the on current only changes moderately after 100 cycles with 100% strain at 1 s per cycle. (fig. S17, E to H), and the mobility is still high at 0.2 $cm^2/V{\cdot}s$ (Fig. 2H and fig. S20). There are no visible cracks in the film after 100 cycles (fig. S21); however, we do observe a slight increase in film roughness (fig. S22), which is known to contribute to decreased mobility (*16*). In comparison, for the neat-**1** film, both the on current and mobility decreased by >3 orders of magnitude after 100 cycles (Fig. 2H and figs. S17, I to K, and S20). Compared to the literature-reported cyclability for semiconductor films (*13*, *16*, *17*), the mobility of our CONPHINE film after cycled stretching is more than 10 times as high, even with twice the strain. Moreover, the CONPHINE film is suitable for long-term usage in practical applications. Although the chain conformation under nanoconfinement has a metastable nature (*31*), the relatively long chain relaxation time allows the film to maintain a similar nanoscale morphology, electrical performance, and stretchability, as was confirmed with a CONPHINE-**1** film after being stored for 1 year (fig. S23).

We fabricated fully stretchable transistors in a bottom-gate–bottom-contact structure, with carbon nanotube (CNT) networks as the electrodes

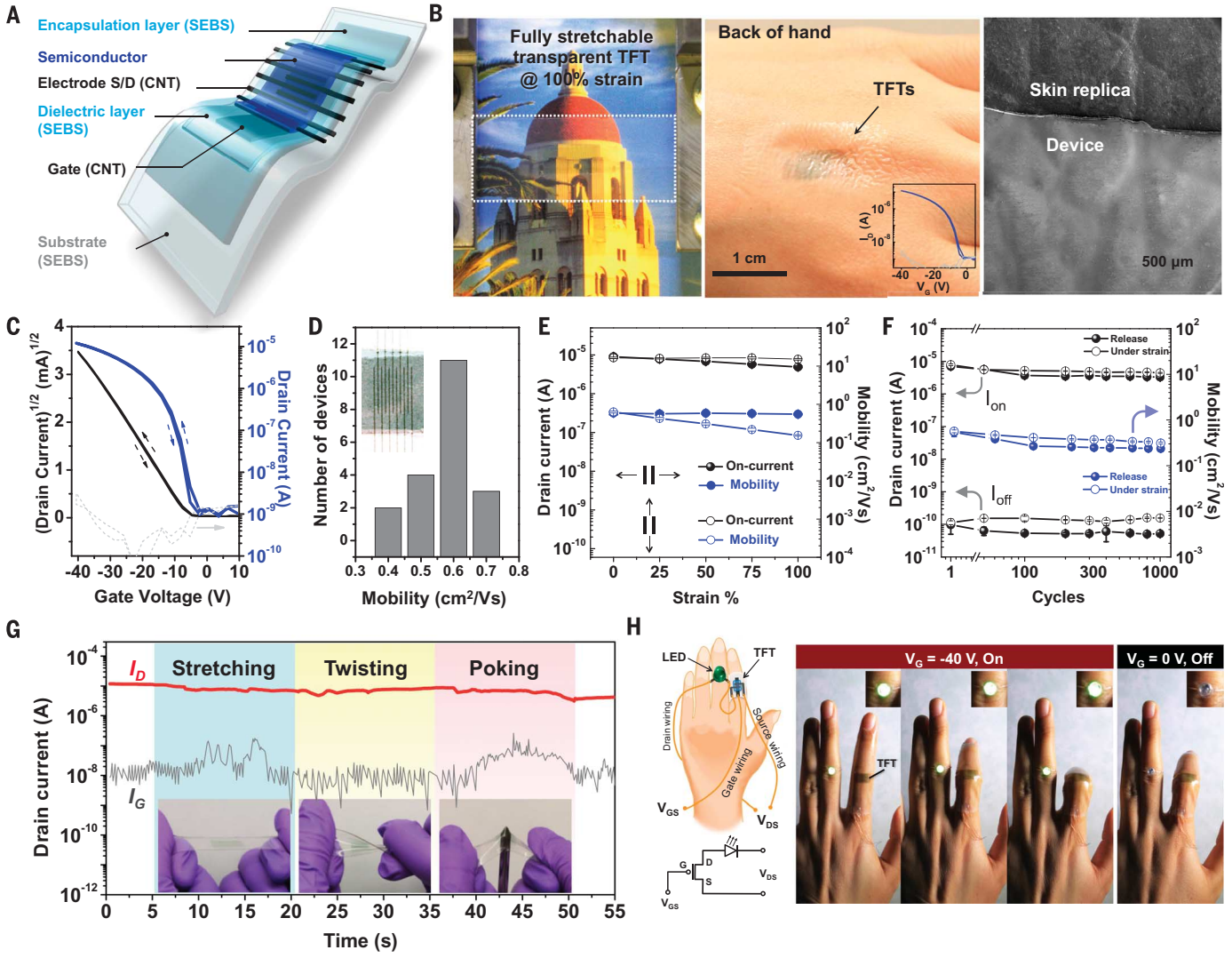

Fig. 3. Fully stretchable transistor fabricated from the CONPHINE-1 film. (**A**) Device structure (channel length: 200 μm; channel width: 4 mm; dielectric capacitance: 15 $\mu F/m^2$). (**B**) Images showing the transistor's transparency (left) and skinlike nature when attached on the back of a hand (middle), with the conformability shown in the SEM image (right). (**C**) A typical transfer curve (V_D = −30 V) at 0% strain. (**D**) Distribution of the mobility from 20 devices in the arrays of fully stretchable transistors (shown with increased contrast in the inset). (**E**) Changes in the on current and mobility [calculated with measured device geometry and dielectric capacitance under strain (table S3); also for the values in (F)] with strains up to 100%, both parallel to (filled circles) and perpendicular to (open circles) the charge transport direction. (**F**) Changes in the on current, off current, and mobility after multiple stretching-releasing cycles (up to 1000 cycles) at 25% strain along the charge transport direction. (**G**) Drain current (I_D) and gate current (I_G) of a fully stretchable TFT under sequential stretching, twisting, and poking with a sharp object. (**H**) Demonstration of the fully stretchable transistor as a finger-wearable driver for an LED.

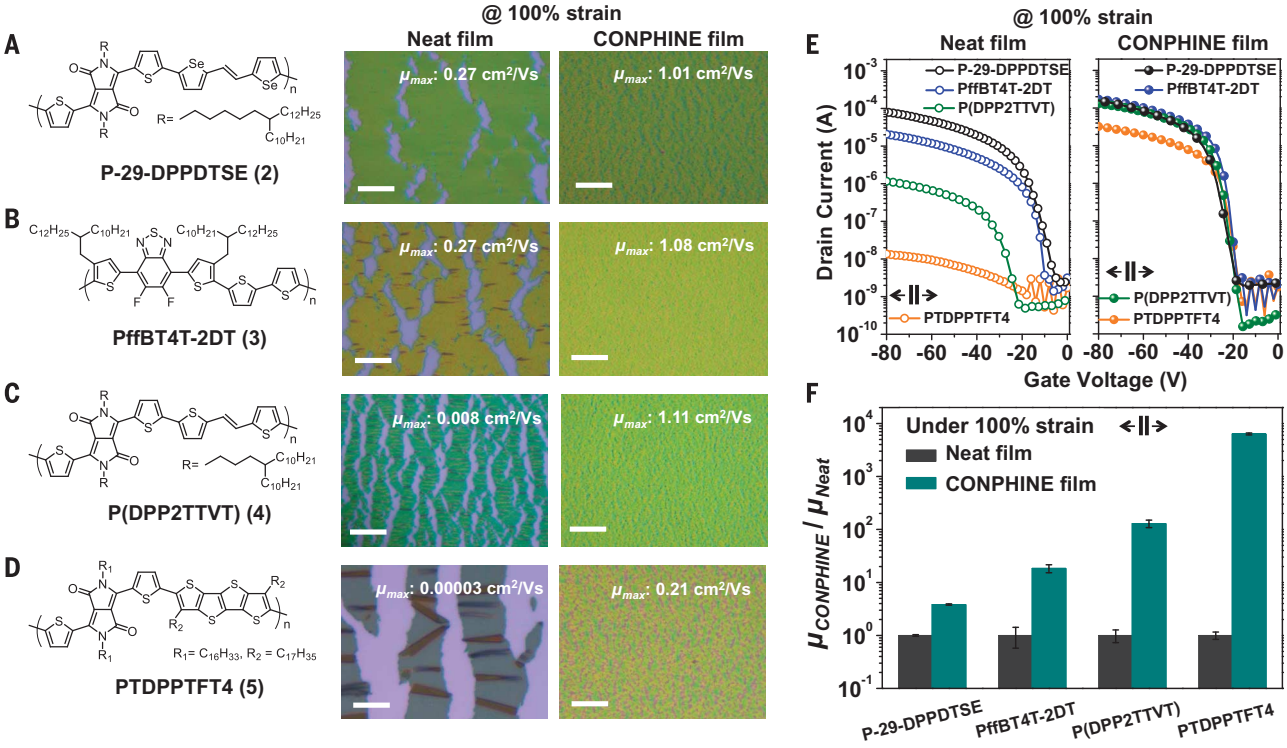

Fig. 4. Applying the CONPHINE method on four distinct conjugated semiconducting polymers to improve their stretchability. (**A** to **D**) Optical micrographs of neat conjugated polymer films (middle) and corresponding CONPHINE films (right) at 100% strain, for polymers of (A) P-29-DPPDTSE (**2**), (B) PffBT4T-2DT (**3**), (C) P(DPP2TTVT) (**4**), and (D) PTDPPTFT4 (**5**), with the chemical structures shown on the left. Scale bar, 20 μm. The CONPHINE films at 100% strain exhibited uneven thicknesses (fig. S29), but no cracks due to plastic deformation. (**E**) Transfer curves (V_D = −80 V) of these neat polymer films (left) and the corresponding CONPHINE films (right) at 100% strain, with the same vertical axis in the two diagrams. (**F**) Normalized mobilities of neat films (gray) and the corresponding CONPHINE films (green) of these conjugated polymers, under 100% strain.

and SEBS as the dielectric layer, stretchable substrate, and encapsulation layer (Fig. 3A and fig. S24). The obtained TFT device has good transparency and excellent conformability for constructing e-skins on human epidermis (Fig. 3B). As shown via a representative transfer curve (Fig. 3C) and output characteristics (fig. S25A), the fully stretchable TFT gives ideal transistor performance and an average mobility of 0.59 $cm^2/V{\cdot}s$ obtained from 20 devices with minimal variations (Fig. 3D). The lower mobility relative to that from the earlier soft contact lamination method is attributed to a higher contact resistance from CNT electrodes compared to Au (fig. S26). When the device is stretched to 100% strain along the charge transport direction, there is only a slight drop in the on current, owing to the increase in channel length from stretching, with the mobility stably maintaining a value of 0.55 $cm^2/V{\cdot}s$ even after being stretched to 100% strain (Fig. 3E, fig. S25B, and table S4). Along the perpendicular direction, the combined effect of the slight decrease in mobility and the device geometric change makes the transfer curve highly stable under strain up to 100% (Fig. 3E and fig. S25C). Moreover, this fully stretchable TFT is highly robust over 1000 repeated stretching cycles to 25% strain at four cycles per second (the general range for applied strains in most wearable electronic applications) (Fig. 3F and fig. S25, D and E). The high stretchability and robustness of the TFT are also revealed by its stable drain current under sequential stretching, twisting, and even poking by a sharp object (Fig. 3G and movie S1). We also attached our transistor, serving as a light-emitting diode (LED) driver, conformably to a human finger to demonstrate its potential use for wearable electronics (Fig. 3H and movie S2).

We applied our CONPHINE method to four other high-performance semiconducting polymers (**2 to 5**), with their chemical structures shown in Fig. 4, A to D (*10*, *13*, *32*) (table S1 and fig. S27). All neat films of these polymers severely crack when subjected to 100% strain (middle column in Fig. 4, A to D), leading to degraded mobilities as shown. Upon using our CONPHINE method, we again obtained nanoconfined morphologies with deformable interfaces (fig. S28). The stretchability of all these films (CONPHINE-**2** to CONPHINE-**5**) is significantly improved, displaying only inhomogeneous deformations at 100% strain (right-column images in Fig. 4, A to D, and fig. S29). As a result, both the on currents and mobilities (values are indicated in their respective images) from these films at 100% strain exceed their neat counterparts by one to four orders of magnitude (Fig. 4, E and F). Notably, four different conjugated polymers (including **1**) are imparted with mobilities >1.0 $cm^2/V{\cdot}s$ at 100% strain.

Polymer nanoconfinement enables high stretchablity in semiconducting materials. In this study, we introduced the CONPHINE method to create conjugated-polymer nanostructures with increased chain dynamics and decreased crystallinity embedded in an elastomer matrix to maintain the mobility during stretching. We anticipate that this general approach will advance the development of stretchable semiconductors for stretchable electronic-skin applications.

REFERENCES AND NOTES

1. D.-H. Kim *et al.*, *Science* **333**, 838–843 (2011).
2. D.-H. Kim *et al.*, *Nat. Mater.* **10**, 316–323 (2011).
3. B. C. K. Tee *et al.*, *Science* **350**, 313–316 (2015).
4. M. Kaltenbrunner *et al.*, *Nature* **499**, 458–463 (2013).
5. Y. Sun, W. M. Choi, H. Jiang, Y. Y. Huang, J. A. Rogers, *Nat. Nanotechnol.* **1**, 201–207 (2006).
6. T. C. Shyu *et al.*, *Nat. Mater.* **14**, 785–789 (2015).
7. H. Lee *et al.*, *Nat. Nanotechnol.* **11**, 566–572 (2016).
8. C. B. Nielsen, M. Turbiez, I. McCulloch, *Adv. Mater.* **25**, 1859–1880 (2013).
9. H. N. Tsao *et al.*, *J. Am. Chem. Soc.* **133**, 2605–2612 (2011).
10. I. Kang, H.-J. Yun, D. S. Chung, S.-K. Kwon, Y.-H. Kim, *J. Am. Chem. Soc.* **135**, 14896–14899 (2013).
11. A. D. Printz, D. J. Lipomi, *Appl. Phys. Rev.* **3**, 021302 (2016).
12. B. Roth *et al.*, *Chem. Mater.* **28**, 2363–2373 (2016).
13. H.-C. Wu *et al.*, *Chem. Mater.* **26**, 4544–4551 (2014).
14. R. Peng *et al.*, *J. Mater. Chem. C Mater. Opt. Electron. Devices* **3**, 3599–3606 (2015).
15. E. Song *et al.*, *Adv. Electron. Mater.* **2**, 1500250 (2016).
16. M. Shin *et al.*, *Adv. Mater.* **27**, 1255–1261 (2015).
17. A. Chortos *et al.*, *Adv. Mater.* **26**, 4253–4259 (2014).

18. B. O'Connor *et al.*, *Adv. Funct. Mater.* **21**, 3697–3705 (2011).
19. J. I. Scott *et al.*, *ACS Appl. Mater. Interfaces* **8**, 14037–14045 (2016).
20. C. M. Stafford, B. D. Vogt, C. Harrison, D. Julthongpiput, R. Huang, *Macromolecules* **39**, 5095–5099 (2006).
21. J. L. Keddie, R. A. L. Jones, R. A. Cory, *Europhys. Lett.* **27**, 59–64 (1994).
22. L. Si, M. V. Massa, K. Dalnoki-Veress, H. R. Brown, R. A. L. Jones, *Phys. Rev. Lett.* **94**, 127801 (2005).
23. J. A. Forrest, K. Dalnoki-Veress, J. R. Dutcher, *Phys. Rev. E Stat. Phys. Plasmas Fluids Relat. Interdiscip. Topics* **56**, 5705–5716 (1997).
24. C. J. Ellison, J. M. Torkelson, *Nat. Mater.* **2**, 695–700 (2003).
25. K. Shin *et al.*, *Macromolecules* **40**, 6617–6623 (2007).
26. J. F. Chang, M. C. Gwinner, M. Caironi, T. Sakanoue, H. Sirringhaus, *Adv. Funct. Mater.* **20**, 2825–2832 (2010).
27. J. Kim *et al.*, *Mater. Lett.* **130**, 227–231 (2014).
28. S. Wang *et al.*, *Proc. Natl. Acad. Sci. U.S.A.* **112**, 10599–10604 (2015).
29. Y. Li, S. P. Singh, P. Sonar, *Adv. Mater.* **22**, 4862–4866 (2010).
30. B. O'Connor *et al.*, *ACS Nano* **4**, 7538–7544 (2010).
31. S. Napolitano, Ed., *Non-Equilibrium Phenomena in Confined Soft Matter* (Springer, 2015).
32. Y. Liu *et al.*, *Nat. Commun.* **5**, 5293 (2014).

ACKNOWLEDGMENTS

J.X., S.W., and Z.B. conceived and designed the experiments; J.X. fabricated the CONPHINE films; J.X., S.W., C.Z., and C.L. fabricated the transistor devices and did the measurements; G.-J.N.W, S.R.-G., B.C.S., Y.-H.K., and H.Y. provided the conjugated polymers; S.L., D.Z., and G.X. performed the glass transition measurement; L.J., Y.W., C.L., and W.C. carried out the mechanical simulations; X.G. did the grazing incidence x-ray diffraction (XRD) characterizations; S.C., V.R.F., and J.W.F.T. did the XPS and scanning electron microscopy (SEM) characterizations; J.P. and R.S. did the scanning transmission electron microscopy characterization; J.Y.O. helped with the film transfer process; S.W., J.X., Z.B., J.W.C., and J.B.-H.T. organized the data and wrote the manuscript; and all authors reviewed and commented on the manuscript. This work is supported by Samsung Electronics (material fabrication and devices) and the U.S. Department of Energy, Office of Science, Basic Energy Sciences, under award DE-SC0016523 (material characterization). S.R.-G. thanks the Fonds de Recherche du Québec: Nature et Technologies for a postdoctoral fellowship. B.C.S. acknowledges the National Research Fund of Luxembourg for financial support (project 6932623). H.Y. thanks the Hong Kong Innovation and Technology Commission for support through ITC-CNERC14SC01. C.L. acknowledges support from the National Science Foundation through CMMI-1553638. Y.-H.K. thanks the NRF Korea (2015R1A2A1A10055620). J.X., Z.B., J.W.C., and Sangyoon Lee are inventors on patent application no. 62/335,250 submitted by Samsung Electronics Co., Ltd., and the board of Trustees of the Leland Stanford Junior University. The GIXD measurements were performed in Advanced Light Source beamline 7.3.3 and SSRL 11-3, which are supported by the director, Office of Science, Office of Basic Energy Sciences, of the U.S. Department of Energy under contract nos. DE-AC02-05CH11231 and DE-AC02-76SF00515, respectively.

SUPPLEMENTARY MATERIALS

www.sciencemag.org/content/355/6320/59/suppl/DC1
Materials and Methods
Tables S1 to S4
Figs. S1 to S29
References (*33*–*47*)
Movies S1 and S2

29 June 2016; accepted 2 December 2016
10.1126/science.aah4496

Science
AAAS

Highly stretchable polymer semiconductor films through the nanoconfinement effect

Jie Xu, Sihong Wang, Ging-Ji Nathan Wang, Chenxin Zhu, Shaochuan Luo, Lihua Jin, Xiaodan Gu, Shucheng Chen, Vivian R. Feig, John W. F. To, Simon Rondeau-Gagné, Joonsuk Park, Bob C. Schroeder, Chien Lu, Jin Young Oh, Yanming Wang, Yun-Hi Kim, He Yan, Robert Sinclair, Dongshan Zhou, Gi Xue, Boris Murmann, Christian Linder, Wei Cai, Jeffery B.-H. Tok, Jong Won Chung and Zhenan Bao (January 5, 2017)

Science **355** (6320), 59-64. [doi: 10.1126/science.aah4496]

Editor's Summary

Trapping polymers to improve flexibility

Polymer molecules at a free surface or trapped in thin layers or tubes will show different properties from those of the bulk. Confinement can prevent crystallization and oddly can sometimes give the chains more scope for motion. Xu *et al.* found that a conducting polymer confined inside an elastomer—a highly stretchable, rubber-like polymer—retained its conductive properties even when subjected to large deformations (see the Perspective by Napolitano).

Science, this issue p. 59; see also p. 24

Science (print ISSN 0036-8075; online ISSN 1095-9203) is published weekly, except the last week in December, by the American Association for the Advancement of Science, 1200 New York Avenue NW, Washington, DC 20005.